


Sequential-measurement thermometry with quantum many-body probes

Yaoling Yang,^{1,*} Victor Montenegro^{1,2,†} and Abolfazl Bayat^{1,2,‡}

¹*Institute of Fundamental and Frontier Sciences, University of Electronic Science and Technology of China, Chengdu 611731, China*

²*Key Laboratory of Quantum Physics and Photonic Quantum Information, Ministry of Education, University of Electronic Science and Technology of China, Chengdu 611731, China*

 (Received 15 March 2024; revised 28 May 2024; accepted 7 August 2024; published 27 August 2024)

Measuring the temperature of a quantum system is an essential task in almost all aspects of quantum technologies. Theoretically, an optimal strategy for thermometry often requires measuring energy, which demands full accessibility over the entire system as well as a complex entangled measurement basis. In this paper, we take a different approach and show that single-qubit sequential measurements in the computational basis not only allow for precise thermometry of a many-body system, but may also achieve precision beyond the thermometry capacity of the probe at equilibrium, given by the Cramér-Rao bound. Thus, using consecutive single-qubit measurements of the probe out of equilibrium is, in most cases, very beneficial, as it achieves lower-temperature uncertainties and avoids demanding energy measurements when compared with probes at thermal equilibrium. To obtain such precision, the time between the two subsequent measurements should be smaller than the thermalization time so that the probe never thermalizes. Therefore, the nonequilibrium dynamics of the system continuously imprint information about temperature in the state of the probe. To demonstrate the generality of our findings, we consider thermometry in both spin chains and the Jaynes-Cummings model.

DOI: [10.1103/PhysRevApplied.22.024069](https://doi.org/10.1103/PhysRevApplied.22.024069)

I. INTRODUCTION

The estimation of temperature, known as thermometry [1,2], holds relevance across all branches of natural sciences [3–8]. To date, its significance becomes increasingly apparent in numerous physical applications, particularly those demanding low-energy excitations within cryogenic environments. Indeed, bringing the system to ultracold temperatures allows us to observe quantum effects or execute precise processing tasks [9]. Hence, a precise thermometry scheme is crucial for determining, for instance, the impact of quantum features in the presence of thermal fluctuations [10,11]. So far, thermometry has been explored in several contexts such as nonlinear optomechanics [12,13], single-particle systems [14–16], solid-state impurity systems [17,18], topological spinless fermions [19], few-fermion thermometry [20], establishing general bounds for optimal nonequilibrium thermometry [21], probe optimization [22–24], global thermometry [25,26], in coupled harmonic oscillators [27], collisional models [28], thermodynamic length [29], critical quantum

thermometry [18,30,31], thermometry enhanced by coherence [32], and ultimate thermometry bounds for arbitrary interactions and measurement schemes [33].

Conventional thermometry relies on the zeroth law of thermodynamics [14], which implies that a probe reaches an equilibrium Gibbs state $\rho(T) = \exp\{-H/(k_B T)\}/\mathcal{Z}$ due to interaction with a thermal reservoir at temperature T . Here, H is the Hamiltonian of the probe, k_B is the Boltzmann constant (hereafter taken as $k_B = 1$), and \mathcal{Z} is the partition function. For any given probe, the best temperature estimation can be obtained by energy measurement, namely, H being the observable to be measured [34,35]. Such measurement yields the ultimate thermometry precision $\text{var}[\hat{T}] \geq T^4/[M(\Delta H)^2]$, where M is the number of measurements, $(\Delta H)^2$ is the energy fluctuations [1,2,34], and $\text{var}[\hat{T}]$ is the variance of the temperature estimator \hat{T} (here, assumed to be unbiased). Estimator \hat{T} maps the measured data into parameter space [36]. In this context, studies on optimal thermometry strategies with coarse-grained measurements have been pursued [16,37] and even beyond standard open-system weak-coupling assumptions [38]. One may focus on finding the optimal probe by engineering Hamiltonian H . Such optimization for a local estimation scheme, where prior information about the temperature is available, results in an effective two-level system with a maximally degenerate excited state [22]. In the

* Contact author: yyaoling@std.uestc.edu.cn

† Contact author: vmontenegro@uestc.edu.cn

‡ Contact author: abolfazl.bayat@uestc.edu.cn

absence of prior information, i.e., global sensing, the optimal probe becomes more complex and extra energy levels are also required [25]. From a practical point of view, the fact that conventional optimal thermometry requires energy measurement makes it very challenging as such actions often require (i) full accessibility over the entire system and (ii) a complex entangled measurement basis. In specific situations, like ferromagnetic states, this approach is not necessary. However, our focus is on more general states. To overcome these challenging requirements, we investigate a metrology scheme applied to thermometry by exploiting sequences of local quantum measurements on the probe at consecutive time intervals [15,39,40].

Quantum measurement and its subsequent wavefunction collapse can be used as means for inducing nonequilibrium dynamics in a many-body system at equilibrium [41–53]. Consecutive local measurements, each separated by a period of nonequilibrium dynamics, provide information about the underlying many-body system that can be used for sensing purposes [15,39,40,54–65]. In a thermometry context, several open questions may arise. Can one achieve precise thermometry through local measurements? If so, can such measurements surpass the precision of conventional optimal thermometry, through exploiting nonequilibrium dynamics? Indeed, a natural question is whether by repeating enough measurements one can reach thermometry precision beyond the generally complex energy measurement in equilibrium probes.

In this work, we estimate the temperature of both a many-body and a light-matter probe. A sequence of consecutive measurements, each followed by a period of nonequilibrium dynamics, is used for estimating the temperature of the system. Three different cases have been studied, namely, weak, strong, and intermediate thermalization regimes. In the intermediate regime, the thermalization rate partially imprints the temperature into the quantum state between consecutive measurements. Consequently, our sequential measurement strategy, in most cases, surpasses the conventional optimal thermometry approach, which measures the entire thermalized probe in the energy basis. We support our claims by analyzing several figures of merit, including bare thermometric sensitivities, scaled thermometry sensitivity per measurement, asymptotic thermometry behavior in the limit of large measurement sequences, as well as the signal-to-noise ratio. To demonstrate the performance of our probe, we have investigated thermometry in both spin chains and the Jaynes-Cummings model.

The rest of the paper is organized as follows. In Sec. II, we introduce the figures of merit for quantum parameter estimation. In Sec. III, we introduce the model of the quantum probes and their open dynamics between the probe and the bath. In Sec. IV, we outline the procedure for sequential measurement sensing. In Sec. V, we study the weak,

intermediate, and strong thermalization regimes. Finally, in Sec. VII, we conclude our work.

II. INFORMATION METRICS

The uncertainty in estimating an unknown parameter λ encoded into a quantum state $\rho(\lambda)$ satisfies the Cramér-Rao inequality [66–70]

$$\text{var}[\hat{\lambda}] \geq \frac{1}{M\mathcal{F}}, \quad (1)$$

where $\text{var}[\hat{\lambda}]$ is the variance of estimator $\hat{\lambda}$ (here, assumed to be unbiased). Estimator $\hat{\lambda}$ assigns a value in the parameter space from the collected measured data [36]. Here M denotes the number of measurement trials and \mathcal{F} stands for the classical Fisher information [71,72]:

$$\mathcal{F} = \sum_j \frac{1}{p_j(\lambda)} [\partial_\lambda p_j(\lambda)]^2. \quad (2)$$

Here $\partial_\lambda := \partial/\partial\lambda$ and the summation \sum_j runs over all j countable measurement outcomes with associate probability $p_j(\lambda) = \text{Tr}[\Upsilon_j \rho(\lambda)]$, where Υ_j is a positive operator-valued measure (POVM) with random outcome j . The classical Fisher information has a well-defined operational meaning, namely, for any fixed measurement basis, the achievable uncertainty is at best lower bounded by the right-hand side of the Cramér-Rao inequality in Eq. (1), with the best scenario achievable if an optimal estimator is employed. See Appendix B for a Bayes estimator.

In single-parameter sensing, the optimal measurement that maximizes the classical Fisher information is termed the quantum Fisher information, denoted $\mathcal{Q} = \max_{\{\Upsilon_j\}}[\mathcal{F}]$ [36]. Hence, by definition, the Cramér-Rao inequality updates to [36,73–76]

$$\text{var}[\hat{\lambda}] \geq \frac{1}{M\mathcal{F}} \geq \frac{1}{M\mathcal{Q}}. \quad (3)$$

The quantum Fisher information \mathcal{Q} , as an optimization procedure over all possible POVMs, can also be formulated in terms of the symmetric logarithmic derivative (SLD) self-adjoint operator $\mathcal{L}(\lambda)$ [36]. This SLD operator is a solution of the Lyapunov equation $2\partial_\lambda \rho(\lambda) = \{\mathcal{L}(\lambda), \rho(\lambda)\}$, where $\{\cdot, \cdot\}$ denotes the anticommutator. In general, it can be proven that the quantum Fisher information can be computed as [36]

$$\mathcal{Q} = \text{Tr}[\rho(\lambda)\mathcal{L}(\lambda)^2] = \text{Tr}[\partial_\lambda \rho(\lambda)\mathcal{L}(\lambda)]. \quad (4)$$

The quantum Fisher information has also a well-defined operational meaning, namely, it represents the ultimate sensing precision achievable to estimate the unknown parameter λ encoded in the quantum probe $\rho(\lambda)$. Note that

to achieve the ultimate level of precision, one must calculate the SLD $\mathcal{L}(\lambda)$ in Eq. (4). However, $\mathcal{L}(\lambda)$ depends on the unknown parameter, and, consequently, the SLD poses significant challenges in local estimation theory, requiring substantial prior information about the unknown parameter [68,77]. This constraint has been addressed in global sensing scenarios [78–80], eliminating the need for prior information about the parameter. Furthermore, even if the optimal measurement is identified, through the eigenstates of the SLD [36], it could be difficult in practice. Hence, a more practical direction can be pursued by exploring sensing with a readily accessible measurement basis.

III. THERMALIZATION PROCESS

To demonstrate that thermometry through local sequential measurements can, under certain conditions, surpass thermometry with probes at thermal equilibrium, we consider two distinct quantum probes following sequential measurement thermometry: the quantum many-body Heisenberg probe and the light-matter Jaynes-Cummings model.

(1) On the one hand, we consider a one-dimensional many-body probe of N interacting spin-1/2 particles with Heisenberg interaction. This is a paradigmatic model in magnetism, explored in both ground-state [81] and nonequilibrium dynamics [82–85]. The Hamiltonian, with open boundary conditions, is

$$H_{\text{Heis.}} = -J \sum_{j=1}^{N-1} \boldsymbol{\sigma}^j \cdot \boldsymbol{\sigma}^{j+1}, \quad (5)$$

where J is the exchange interaction between particles and $\boldsymbol{\sigma}^j$ is a vector composed of Pauli matrices $\boldsymbol{\sigma}^j = (\sigma_x^j, \sigma_y^j, \sigma_z^j)$ at site j . Note that spin components obey $[\sigma_\alpha^n, \sigma_\beta^m] = 2i\delta_{nm}\epsilon_{\alpha\beta\theta}\sigma_\theta^j$, where $(\alpha, \beta, \theta = x, y, z)$, δ_{nm} is the Kronecker delta, and $\epsilon_{\alpha\beta\theta}$ is the Levi-Civita symbol. Without loss of generality, we consider the ferromagnetic scenario throughout our work, wherein $J > 0$. In this scenario, the energy is minimized when the spins are parallel to each other, with the triplet state favoured.

(2) On the other hand, we consider a single two-level atom interacting with a single-mode quantized electromagnetic field via the Jaynes-Cummings Hamiltonian (in Planck units)

$$H_{\text{JC}} = \omega_0 a^\dagger a + \omega_0 \frac{\sigma_z}{2} + \Omega (a^\dagger \sigma_- + a \sigma^+), \quad (6)$$

where we have assumed a resonance frequency ω_0 between the two-level atom and the field, Ω is the light-matter coupling strength, a (a^\dagger) is the annihilation (creation) bosonic operator, and $\sigma_- = |g\rangle\langle e|$ ($\sigma_+ = \sigma_-^\dagger$) is the lowering (raising) two-level atom operator with $|e\rangle$ and $|g\rangle$ the

excited and ground states of the two-level atom, respectively. Moreover, we have performed the rotating-wave approximation; namely, we have discarded fast oscillating terms in the Hamiltonian, which is an approximation valid in the weak coupling regime $\Omega \lesssim 0.1\omega_0$ [86]. The Jaynes-Cummings Hamiltonian is a paradigmatic model of light-matter interactions that can be exactly solved in the polariton basis $\{|g, n+1\rangle, |e, n\rangle\}$, where n is the field number state $a^\dagger a |n\rangle = n|n\rangle$.

To simulate the open dynamics between the quantum probes and the bath, we consider a master equation in the Born-Markov approximation as—*later demonstrated within this section*—its steady state guarantees the true probe’s thermalization [87–92], given by

$$\begin{aligned} \dot{\rho}(t) = & -i[H_S, \rho(t)] \\ & + \sum_{\nu>0}^N \kappa(\nu) \left[A(\nu)\rho(t)A^\dagger(\nu) - \frac{1}{2}\{A^\dagger(\nu)A(\nu), \rho(t)\} \right] \\ & + \sum_{\nu>0}^N \kappa(-\nu) \left[A^\dagger(\nu)\rho(t)A(\nu) - \frac{1}{2}\{A(\nu)A^\dagger(\nu), \rho(t)\} \right]. \end{aligned} \quad (7)$$

In the above, for its derivation [87], it is considered the usual treatment of having the Hamiltonian of the total closed system as [93]

$$H = H_S + H_E + H_{S,E}, \quad (8)$$

where H_S is the system’s Hamiltonian under study, H_E is the Hamiltonian of the environment, and $H_{S,E}$ is the Hamiltonian of the interaction between the system’s Hamiltonian and the environment. The latter is taken to be of the form $H_{S,E} = A \otimes R$, where A and R are self-adjoint operators acting on the system and the reservoir Hilbert spaces, respectively [87]. One can obtain

$$A(\nu) = \sum_{\varepsilon' - \varepsilon = \nu} P(\varepsilon) A P(\varepsilon'), \quad (9)$$

where $P(\varepsilon)$ is the projector onto the eigenspace corresponding to the eigenvalue ε of the system’s Hamiltonian, and the sum runs over all the Bohr frequencies relative to the system’s Hamiltonian [87]. Finally,

$$\kappa(-\nu) = \exp\left(-\frac{\nu}{T}\right)\kappa(\nu) \quad (10)$$

is known as the Kubo-Martin-Schwinger (KMS) condition [87,88] that ensures that the steady state of the master equation (7) corresponds to the Gibbs state. Note that $\kappa(\nu)$ is generally computed as a function of the correlation function of the bath [88]. Here, however, we assume that $\kappa(\nu)$

is a free parameter defined by a constant value κ and thus $\kappa(-\nu) = \exp(-\nu/T)\kappa$.

Three approximations have been made to obtain the above master equation: the Born approximation (assuming weak system-reservoir interaction coupling), the Markovian approximation (neglecting memory effects of the reservoir on the system due to a coarse graining in time of the system-reservoir dynamics), and the rotating-wave approximation [87]. In particular, it is worth emphasizing that the rotating-wave approximation is applicable in the above open quantum dynamics when the maximum of the rates $\kappa(\nu)$ is significantly smaller than the minimum difference between the Bohr frequencies relative to the system's Hamiltonian [87,93]:

$$\kappa_{\max} \ll \Delta\nu_{\min}. \quad (11)$$

In what follows, we have carefully checked the above approximations in our numerical simulations, specifically Eq. (11), which can be numerically tractable for both models.

On the one hand, we consider the Jaynes-Cummings model to exchange excitations with the bath only through the bosonic mode (i.e., we neglect losses in the two-level system). In this manner, the system-reservoir Hamiltonian interaction is

$$H_{S,E}^{(JC)} = (a^\dagger + a) \sum_k g_k (b_k + b_k^\dagger), \quad (12)$$

where mode a interacts with an infinite number of reservoir modes b_k with corresponding coupling strength g_k . Here, we identify $A_{JC} = A = (a^\dagger + a)$, and thus the master equation for the Jaynes-Cummings model is the same as that presented in Eq. (7), with quantum jump operator

[87–92]

$$\begin{aligned} A_{JC}(\nu = \epsilon_m - \epsilon_n) &= A(\nu = \epsilon_m - \epsilon_n) \\ &= |\epsilon_n\rangle\langle\epsilon_n|(a^\dagger + a)|\epsilon_m\rangle\langle\epsilon_m|, \end{aligned} \quad (13)$$

where $H_{JC}|\epsilon_l\rangle = \epsilon_l|\epsilon_l\rangle$ and $\nu = \epsilon_m - \epsilon_n > 0$ is the Bohr transition frequency from energy level ϵ_n to ϵ_m . This gives rise to a closed form of the master equation found in Ref. [87], where quantum jumps occur between the entire energy ladder of the Jaynes-Cummings Hamiltonian. Note that the open dynamics is valid for $\kappa_{\max} \ll 2\Omega$ (rotating-wave approximation validity), since the typical evolution timescale of the system is given by the inverse of the Rabi frequency 2Ω [87].

On the other hand, we consider the Heisenberg model exchanging excitations with the bath through local spin relaxation (i.e., each qubit is individually coupled to a common bath). Interestingly, the scenario involving two coupled qubits interacting with common and separate baths has been addressed in Ref. [89]. Motivated by the above JC scenario of two coupled qubits in contact with a common bath, we consider a single-qubit dissipation of the form

$$H_{S,E}^{(\text{Heisenberg})} = (\sigma^+ + \sigma^-) \sum_{k=1}^{\infty} \tilde{g}_k (b_k^\dagger + b_k) \quad (14)$$

with \tilde{g}_k the coupling strength between a single qubit and the bath. Here, we identify $A_{\text{Heis.}} = A' = (\sigma^+ + \sigma^-)$. Hence, the quantum jump operator $A'(\eta)$ can be written in the form [87–89]

$$\begin{aligned} A_{\text{Heis.}}(\eta = \epsilon_m - \epsilon_n) &= A'(\eta = \epsilon_m - \epsilon_n) \\ &= |\epsilon_n\rangle\langle\epsilon_n|(\sigma^+ + \sigma^-)|\epsilon_m\rangle\langle\epsilon_m|, \end{aligned} \quad (15)$$

where $H_{\text{Heis.}}|\epsilon_l\rangle = \epsilon_l|\epsilon_l\rangle$ ($l = 0, 1, \dots, 2^N$) and $\eta = \epsilon_m - \epsilon_n > 0$ is the Bohr transition frequency from energy level ϵ_n to ϵ_m . Therefore, we heuristically extend the losses across the whole spin chain following the master equation:

$$\begin{aligned} \dot{\rho}(t) &= -i[H_{\text{Heis.}}, \rho(t)] + \sum_{\substack{j=1 \\ \eta>0}}^N \kappa(\eta) \left[A'_j(\eta) \rho(t) A_j^{\dagger}(\eta) - \frac{1}{2} \{A_j^{\dagger}(\eta) A'_j(\eta), \rho(t)\} \right] \\ &\quad + \sum_{\substack{j=1 \\ \eta>0}}^N \kappa(-\eta) \left[A_j^{\dagger}(\eta) \rho(t) A'_j(\eta) - \frac{1}{2} \{A'_j(\eta) A_j^{\dagger}(\eta), \rho(t)\} \right] \end{aligned} \quad (16)$$

with the index j running over all spin sites. Note that Eq. (16) is not a rigorous mathematical derivation of the quantum open dynamics of the Heisenberg probe. A more rigorous Lindbladian might be constructed using the

procedure shown in Ref. [94] or by extending the results derived for the coupled two-qubit case addressed in Ref. [89]. However, it is a simple and intuitive extension meant to represent local spin losses in a system of N

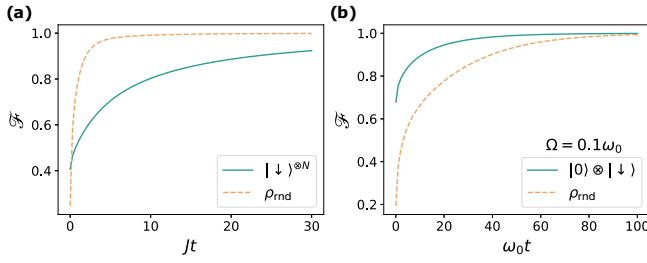


FIG. 1. (a) The fidelity \mathcal{F} between the Gibbs state ρ_{th} and the evolved state for the Heisenberg model as a function of time Jt . We set $\kappa = 0.5J$, $T = J$, and the system size is fixed at $N = 4$. (b) The fidelity \mathcal{F} between the Gibbs state ρ_{th} and the evolved state for the Jaynes-Cummings model as a function of time t . We set $\kappa = 0.05\omega_0$, $\Omega = 0.1\omega_0$, and $T = \omega_0$. Two initial states are considered: a ground state and a random state for both figures.

interacting particles. Since the rigor of the master equation lies beyond the scope of our work, we consider the above master equation as it still ensures the Gibbs state as its steady state.

To demonstrate that master equations (7) and (16) effectively thermalize the system into the correct Gibbs state, we evaluate the fidelity \mathcal{F} [95] between the Gibbs state $\rho_{\text{th}} = e^{-H/T}/\mathcal{Z}$ and a state evolving under the open dynamics. In Fig. 1(a), we plot the fidelity \mathcal{F} between ρ_{th} and $|\psi\rangle = |\downarrow\rangle^{\otimes N}$ and a randomly generated initial state ρ_{rnd} (spanned in the computational basis) as a function of time for the Heisenberg scenario. Without loss of generality, we consider $\kappa = 0.5J$, $T = J$, and the system size $N = 4$. As the figure shows, the fidelity approaches unity for both initial states; therefore, the open dynamics thermalizes into the correct Gibbs state of the system. In Fig. 1(b), we plot the fidelity \mathcal{F} between ρ_{th} and $|\psi\rangle = |\downarrow, 0\rangle$, and a randomly generated initial state ρ_{rnd} (spanned in the polariton basis) as a function of time for the Jaynes-Cummings scenario. As observed from the figure, the system consistently reaches its steady state corresponding to the correct Gibbs state. Note that the steady-state solution can also be verified directly in the Markovian master equation. See Appendix A for details on the Heisenberg probe case and Ref. [87] for the Jaynes-Cummings model.

With these settings, we identify three regimes of thermalization, namely, (i) the weak thermalization regime, (ii) the intermediate thermalization regime, and (iii) the strong thermalization regime. Each case will be addressed using sequential measurement thermometry in the following sections.

IV. SEQUENTIAL MEASUREMENT SENSING PROTOCOL

The standard approach to estimating an unknown parameter, such as temperature, involves conducting a single measurement on each identical copy of the probe to

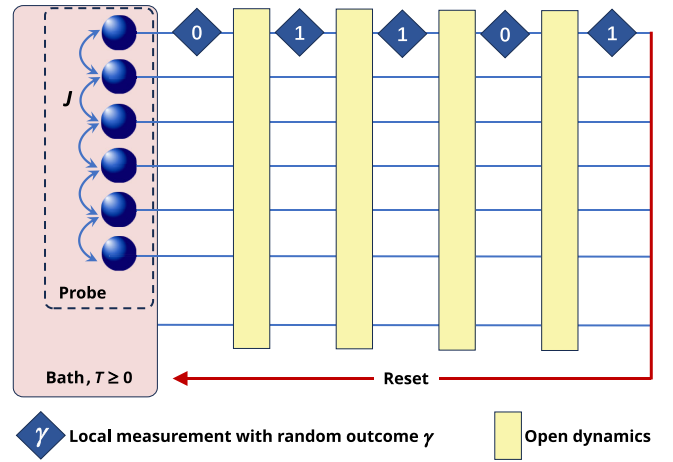


FIG. 2. Sketch of the sequential measurement metrology adapted for thermometry purposes, in particular, for a quantum many-body probe with exchange interaction J initialized at thermal equilibrium with a bath at an unknown temperature T . A finite number of local sequential measurements n_{seq} is performed on the probe, followed by the probe-bath open evolution, collecting correlated measurement outcomes. Here, the single quantum trajectory $\boldsymbol{\gamma}_1$ collects five measurement outcomes $\boldsymbol{\gamma}_1 = (0, 1, 1, 0, 1)$ corresponding to $n_{\text{seq}} = 5$. After a certain number of sequential measurements is performed on the probe, the system is reset for a new quantum trajectory.

construct probability distributions. Once the probability distributions are determined, one can evaluate the classical Fisher information, as shown in Eq. (2). Here, we adopt a different sensing approach, where a sequence of measurements is performed on the probe before restarting the system for a new run of sequential measurements. This sensing protocol collects correlated measurement outcomes, which reduces the number of identical copies of the probe (or the total protocol time) to achieve (or surpass) the same level of sensing precision, thus using the sensing resources significantly more efficiently [39,40]. Upon conducting a local measurement on the probe, the quantum state of the entire system collapses, effectively creating another probe that evolves during a successive time interval. The steps of the sequential measurement sensing procedure are as follows; see Fig. 2.

- (i) A quantum probe evolves according to Eq. (16) from $\rho^{(j)}(0)$ to $\rho^{(j)}(\tau_j)$.
- (ii) At time τ_j , projective measurements $\{\Pi_{\gamma_j}\}$ with random outcome γ_j are performed on the probe, collapsing the state into

$$\rho^{(j+1)}(0) = \frac{\Pi_{\gamma_j} \rho^{(j)}(\tau_j) \Pi_{\gamma_j}^\dagger}{p(\gamma_j)}, \quad (17)$$

where

$$p(\gamma_j) = \text{Tr}[\Pi_{\gamma_j} \rho^{(j)}(\tau_j) \Pi_{\gamma_j}^\dagger] \quad (18)$$

is the probability associated with γ_j at step j .

(iii) The random outcome γ_j is recorded and the new initial state $\rho^{(j+1)}(0)$ is replaced in (i).

(iv) The above steps are repeated until n_{seq} measurement outcomes are consecutively obtained.

(v) After gathering a data sequence of length n_{seq} , i.e., $\boldsymbol{\gamma}^{(n_{\text{seq}})} = (\gamma_1, \dots, \gamma_{n_{\text{seq}}})$, the probe is reset to $\rho_0^{(j)}$ and the process is repeated to generate a new trajectory.

The above steps show that one effectively deals with different probes at each measurement step. Unlike standard sensing schemes [96–99], there is no requirement for specific maximally entangled probes, the necessity for exploiting quantum phase transitions, or quantum control. One recovers the standard sensing scheme by setting $n_{\text{seq}} = 1$.

In the context of the sequential measurement sensing scenario, the relevant figure of merit is the classical Fisher information that accounts for the total information content provided by all possible quantum trajectories [40], namely,

$$\mathcal{F}^{(n+1)} = \mathcal{F}^{(n)} + \Delta\mathcal{F}^{(n+1)}, \quad (19)$$

where $\mathcal{F}^{(n)}$ is the classical Fisher information at measurement step n , and $\Delta\mathcal{F}^{(n+1)}$ is the classical Fisher information increment after an additional measurement has been performed on the probe, that is,

$$\Delta\mathcal{F}^{(n+1)} := \sum_{\boldsymbol{\gamma}^{(n)}} P_{\boldsymbol{\gamma}^{(n)}} f^{\boldsymbol{\gamma}^{(n)}}. \quad (20)$$

Here, $\sum_{\boldsymbol{\gamma}^{(n)}}$ runs over all possible quantum trajectories of length n , $f^{\boldsymbol{\gamma}^{(n)}}$ is the classical Fisher information obtained from the $(n+1)$ th sequential measurement probability distribution in a particular quantum trajectory of length n , i.e., $\boldsymbol{\gamma}^{(n)}$, and

$$P_{\boldsymbol{\gamma}^{(n)}} = \prod_{j=1}^n p(\gamma_j) \quad (21)$$

is the conditional probability associated with the trajectory. Note that while Eq. (19) is the exact classical Fisher information for the sequential measurement sensing case, the exponential growth in computing all probability distributions limits the exact evaluation to $n_{\text{seq}} \sim 20$. To explore the sensing capabilities of the probe for large values of n_{seq} , we employ the Monte Carlo methodology developed in Ref. [40] to evaluate Eq. (19), where the most

likely probability distributions are naturally selected. This approximation yields

$$\Delta\mathcal{F}^{(n)} \sim \frac{1}{\mu} \sum_{j=1}^{\mu} \mathcal{F}^{j,(n)}, \quad (22)$$

where $\mathcal{F}^{j,(n)}$ represents the classical Fisher information obtained from $p(\gamma_n)$ in Monte Carlo trajectory j at measurement step n , and μ accounts for the total number of Monte Carlo samples.

V. SEQUENTIAL MEASUREMENT THERMOMETRY

The probe's initialization, i.e., before any measurement is performed on the probe, is adequately described by the Gibbs state

$$\rho(T) = \frac{e^{-H/T}}{\mathcal{Z}(T)}, \quad (23)$$

where H is the system Hamiltonian, T is the temperature to be estimated, and $\mathcal{Z}(T) = \text{Tr}[e^{-H/T}]$ is the partition function.

Note that it has been shown that the SLD for the probe at thermal equilibrium in Eq. (23) is $\mathcal{L} = T^{-2}(H - \langle H \rangle)$ [2]. Therefore, the quantum Fisher information reduces to

$$\mathcal{Q} = \frac{1}{T^4} (\Delta H)^2, \quad (24)$$

where $(\Delta H)^2 = \langle H^2 \rangle - \langle H \rangle^2$ is the energy fluctuations. This relates directly to the heat capacity of the system, denoted

$$C_T := \partial_T \langle H \rangle = \frac{1}{T^2} (\Delta H)^2. \quad (25)$$

Consequently, it can also be demonstrated that the most informative measurements regarding temperature T in Eq. (23) are measurements in the energy basis that often require full accessibility to the entire system [34]. However, from a practical standpoint, having access to the whole system and energy measurements is not readily available. Therefore, determining the thermometry capabilities of a more minimalist approach, in which only local measurements are performed on a single qubit in the computational basis, is highly desirable. In what follows, we have all the ingredients to explore three relevant regimes of thermalization between the probe and the bath using a sequential measurement thermometry approach. In addition, we put forward a fair comparison between the sequential and optimal thermometry strategies using several figures of merit, particularly the rescaled thermometry sensitivity per measurement and the asymptotic behavior of the sequential thermometry strategy.

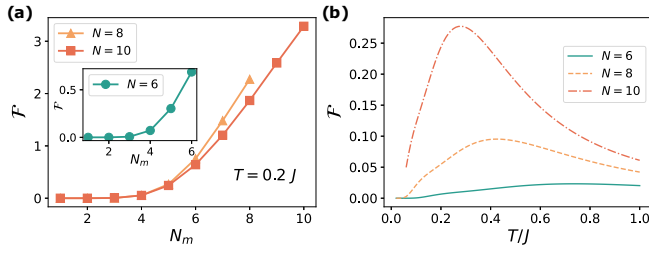


FIG. 3. (a) The classical Fisher information \mathcal{F} as a function of the number of measured qubits N_m for various system sizes N for a fixed temperature $T = 0.2J$. (b) The classical Fisher information \mathcal{F} as a function of temperature T when measuring half of the system for various system sizes N .

A. Strong thermalization regime

Since the Heisenberg model allows us to derive analytical closed forms for the quantum Fisher information of the first nontrivial case, we focus solely on investigating this scenario. However, similar conclusions can be drawn from the Jaynes-Cummings model (or any other probe) in situations of strong thermalization. Indeed, in this case, the probe becomes strongly thermalized between consecutive measurements. Thus, an approximation of the above is to consider the quantum many-body probe at thermal equilibrium. Specifically, sequential measurement thermometry with $n_{\text{seq}} = 1$, as a subsequent measurement will be performed on an identical copy of the probe due to its strong thermalization with the bath.

In Fig. 3(a), we plot the classical Fisher information \mathcal{F} as a function of the number of adjacent measured qubits N_m at fixed temperature $T = 0.2J$. The measurements are performed in the computational basis. As shown in the figure, the Fisher information \mathcal{F} increases nonlinearly with an increasing number of measured qubits. It is worth noting that local measurement on a single qubit $N_m = 1$ gives zero Fisher information. Therefore, there exists a neces-

sity to consider $N_m > 1$ for estimation purposes. The null classical Fisher information is due to the symmetries of the Heisenberg probe at thermal equilibrium. One can straightforwardly demonstrate that the reduced density matrix of a single qubit is the identity, and thus there is no dependence on the temperature whatsoever. This situation is different from the later-discussed Jaynes-Cummings model at thermal equilibrium, where the reduced density matrix of the qubit does depend on the temperature. In Fig. 3(b), we plot the classical Fisher information \mathcal{F} as a function of temperature T when measuring half of the system in the computational basis. As the figure shows, the Fisher information tends to vanish in two extreme cases: $T \rightarrow 0$ and $T \rightarrow \infty$, regardless of the system size. The value remains significantly smaller compared to the scenario of measuring more particles, as shown in Fig. 3(a).

To determine the ultimate sensing precision of the probe, we evaluate the quantum Fisher information as [see Eqs. (24) and (25)]

$$\mathcal{Q} = \frac{1}{T^2} C_T = \frac{1}{T^2} \partial_T \langle H \rangle, \quad (26)$$

where we have used the heat capacity shown in Eq. (25). While obtaining general analytical results for $\langle H \rangle$ and \mathcal{Q} for the Heisenberg spin chain at thermal equilibrium poses challenges, it is possible to address the trivial case of $N = 2$ and the first nontrivial scenario of $N = 3$ ($N = 4$ is also possible to obtain an analytical result, yet it is excessively cumbersome to provide any useful insight):

$$\langle H \rangle = \begin{cases} \frac{4J}{3e^{4J/T} + 1} - J & \text{for } N = 2, \\ \frac{4J(1 - e^{6J/T})}{e^{4J/T} + 2e^{6J/T} + 1} & \text{for } N = 3, \end{cases}$$

and

$$\mathcal{Q} = \begin{cases} 12J^2 T^{-4} \left[\sinh\left(\frac{2J}{T}\right) + 2 \cosh\left(\frac{2J}{T}\right) \right]^{-2} & \text{for } N = 2, \\ \frac{8J^2 e^{4J/T} (9e^{2J/T} + e^{6J/T} + 2)}{T^4 (e^{4J/T} + 2e^{6J/T} + 1)^2} & \text{for } N = 3. \end{cases}$$

Given that the behavior of \mathcal{Q} remains universal regardless of the choice of N , the expressions presented for $N = 2$ and $N = 3$ suffice to provide significant insight.

In Fig. 4(a), the quantum Fisher information of the Gibbs state in Eq. (23) is plotted as a function of the temperature T for various system sizes N . As the figure shows, the quantum Fisher information increases with

the system size N . This implies that the inherent nature of the many-body probe enhances thermometric capabilities. To understand the behavior of the quantum Fisher information for the Heisenberg spin chain at thermal equilibrium, one can examine the average energy as the system size increases under two extreme temperature limits, namely, $T \rightarrow 0$ and $T \rightarrow \infty$. The former case involves the ground state of the system, resulting in an average

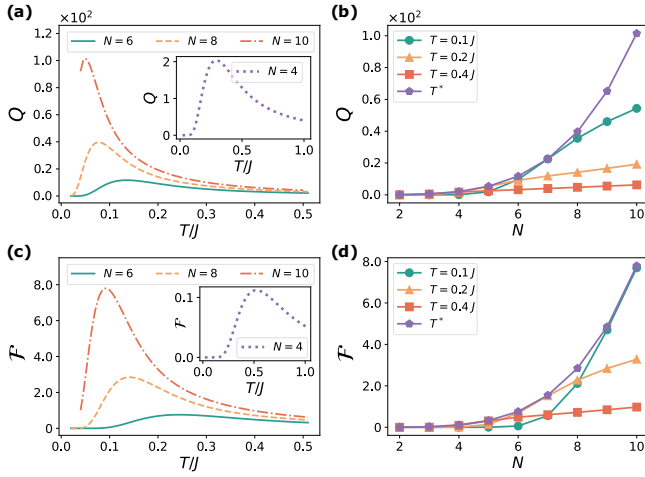


FIG. 4. (a) Quantum Fisher information \mathcal{Q} as a function of temperature T for several system sizes N . (b) Quantum Fisher information \mathcal{Q} as a function of the system size N for several temperatures T . (c) Classical Fisher information \mathcal{F} as a function of temperature T for various system sizes N . (d) Classical Fisher information \mathcal{F} as a function of system size N for different temperatures T .

energy of $\langle H \rangle = -J(N-1)$, while the latter scenario yields an asymptotic value of $\langle H \rangle \rightarrow 0$. The transition between these two limits gives rise to an inflection point and, consequently, to the peak observed in the quantum Fisher information. As the average energy of the ground state decreases with increasing system size N , the rate for which the transition between these two extreme cases occurs becomes more pronounced. Consequently, the quantum Fisher information increases significantly, yet maintaining the same behavior. Note that in these two limits, $T \rightarrow 0$ and $T \rightarrow \infty$, the quantum Fisher information becomes effectively independent of the unknown parameter T (i.e., $\mathcal{Q} \rightarrow 0$). However, the quantum Fisher information reaches its maximum at low-temperature values. A temperature range highly relevant from a practical perspective.

In Fig. 4(b), the quantum Fisher information is presented as a function of the system size N for various temperature values T . As evident from the figure, a fixed temperature T leads to a consistent increase in the quantum Fisher information, implying that spin chains with a larger number of particles indeed contribute to enhanced thermometry. Interestingly, the maximum quantum Fisher information with respect to temperature, denoted $\mathcal{Q}_{\max} = \mathcal{Q}(T = T^*)$, for a given N exhibits a clear nonlinear behavior as the system size increases. This scenario is particularly valuable for local estimation theory, where significant prior information with respect to the unknown parameter is available.

To extract all the information content about the temperature, one needs to perform measurements in the energy

basis of the entire spin chain, as defined in Eq. (23) [34]. However, gaining access to and resolving the complete spectra of the Heisenberg spin chain is often infeasible. Therefore, we evaluate the classical Fisher information using a suboptimal yet accessible measurement basis:

$$\Pi_{\gamma^{(N)}} = \bigotimes_{j=1}^N \frac{\mathbb{I}_j + (-1)^{\gamma_j} \sigma_z^j}{2}, \quad \gamma_j = 0 \text{ or } 1. \quad (27)$$

Using this measurement basis, it becomes straightforward to calculate all the probabilities associated with measurement outcomes $\gamma^{(N)} = (\gamma_1, \gamma_2, \dots, \gamma_N)$ from $(0_1, 0_2, \dots, 0_N)$ to $(1_1, 1_2, \dots, 1_N)$, and, subsequently, determine the corresponding classical Fisher information.

In Fig. 4(c), the classical Fisher information is plotted as a function of temperature T for various system sizes N . As the figure shows, the advantages of utilizing a Heisenberg many-body thermometry persist even with this suboptimal measurement basis. In addition, the behavior of the classical Fisher information mirrors that observed for the quantum Fisher information, although with a reduced factor of approximately 10.

In Fig. 4(d), we present the classical Fisher information as a function of the system size N for various temperatures T . Similar to the quantum Fisher information discussed earlier, we denote by $\mathcal{F}_{\max} = \mathcal{F}(T = T^*)$ the maximum classical Fisher information with respect to the temperature for a given N . As observed in the figure, with the suboptimal measurement basis considered in this context, a distinct nonlinear increase occurs with the increase of the system size.

As discussed above, the strong thermalization regime is constrained to the probe's heat capacity. In our case, the heat capacity of the quantum many-body probe increases with the system size, yet takes no advantage of the sequential measurement thermometry scheme as the probe in between measurements is strongly thermalized once again into a Gibbs state, thus corresponding to an effective copy of the probe's initial state.

B. Weak thermalization regime

For this regime of thermalization, one can approximate the quantum probe to evolve in the limit of vanishingly weak probe thermalization, namely, when the Gibbs state evolves according to the unitary time operator $U(\tau) = e^{-i\tau H}$ (in Planck units, $\hbar = 1$) between consecutive measurements.

For the Heisenberg many-body probe, without loss of generality, we measure a local spin at site N via

$$\Pi_{\gamma_j}^{(N)} = \frac{\mathbb{I}_N + (-1)^{\gamma_j} \sigma_z^N}{2}, \quad \gamma_j = 0 \text{ or } 1, \quad (28)$$

undergoing a fixed evolution time $J\tau = N$ between consecutive measurements. The choice of the time scale $J\tau =$

N in between sequential measurements is considered only to ensure that local correlations have enough time to spread throughout the system.

In Fig. 5(a), we plot the classical Fisher information \mathcal{F} as a function of the number of sequential measurements n_{seq} for various system sizes N and a fixed temperature $T = 0.3J$. As seen from the figure, a noticeable increase in the classical Fisher information is evident for a small number of sequences $n_{\text{seq}} \sim 10$. Subsequently, the classical Fisher information grows significantly slower as the number of sequences increases, indicating that the information gain with respect to temperature becomes weaker. To understand this behavior, we calculate the von Neumann entropy of the entire system, averaged over a total of μ Monte Carlo trajectories, as

$$\bar{\mathcal{S}} = \frac{1}{\mu} \sum_{j=1}^{\mu} \mathcal{S}_j, \quad (29)$$

where

$$\mathcal{S}_j = -\text{Tr} \left[\rho_j^{(n_{\text{seq}})} \log \rho_j^{(n_{\text{seq}})} \right] \quad (30)$$

is the von Neumann entropy computed for state $\rho_j^{(n_{\text{seq}})}$, which is the density matrix for trajectory j where n_{seq} measurements have been performed on the probe. In Fig. 5(b), we plot the averaged entropy $\bar{\mathcal{S}}$ as a function of the number of sequences n_{seq} for various system sizes N and the given temperature $T = 0.3J$. As observed in the figure, the averaged entropy decreases monotonically for all cases, starting from a highly mixed state and converging towards zero, indicating a pure state $\bar{\mathcal{S}} = 0$. Hence, the system undergoes purification with each measurement performed on the probe [100]. As the system size increases, the cost of purifying the system also rises.

In the Jaynes-Cummings model, similar conclusions can be drawn when the system undergoes sequential measurements during unitary evolution. The sequential measurement thermometry in this case will be carried out by measuring the (qubit) two-level atom at regular times. In Fig. 5(c), the classical Fisher information \mathcal{F} is plotted as a function of the number of sequential measurements n_{seq} for a fixed temperature $T = 0.3\omega_0$. The figure clearly shows that the classical Fisher information saturates with an increasing number of sequential measurements on the Jaynes-Cummings probe. In Fig. 5(d), the average von Neumann entropy is plotted against n_{seq} for the same temperature $T = 0.3\omega_0$. The figure shows that the system quickly becomes pure, thus losing information content about the temperature that was originally encoded in the Jaynes-Cummings quantum state. This behavior can be understood by considering that the Jaynes-Cummings dynamics are constrained to transitions within the polariton

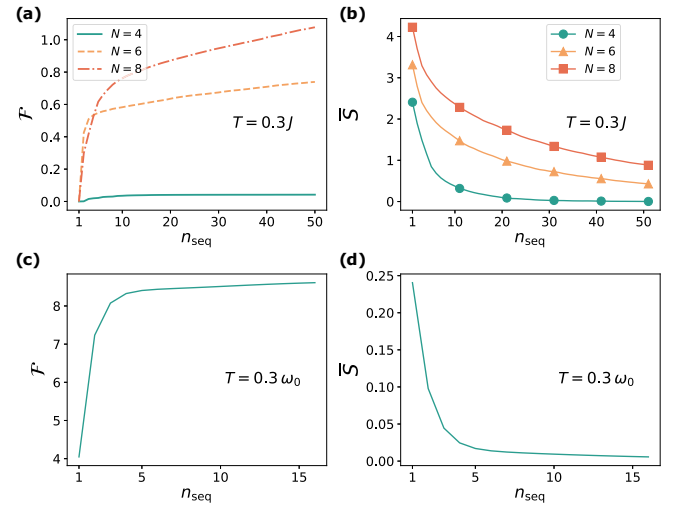


FIG. 5. Heisenberg probe: (a) classical Fisher information \mathcal{F} as a function of n_{seq} for various system sizes N and fixed $T = 0.3J$, (b) averaged von Neumann entropy $\bar{\mathcal{S}}$ as a function of n_{seq} for different N and fixed $T = 0.3J$. We consider $J\tau = N$. Jaynes-Cummings probe: (c) classical Fisher information \mathcal{F} as a function of n_{seq} at $T = 0.3\omega_0$, (d) averaged von Neumann entropy $\bar{\mathcal{S}}$ as a function of n_{seq} for a given $T = 0.3\omega_0$. We consider $\Omega = 0.1\omega_0$ and $\omega_0\tau = 20$.

basis $\{|g, n+1\rangle, |e, n\rangle\}$. The evolution of the system (considered pure for the sake of explanatory simplicity) can be described by a correlated state of the form $|\psi(t)\rangle_{\text{JC}} \sim \mathcal{A}_e(n)|e, n\rangle + \mathcal{A}_g(n)|g, n+1\rangle$, where $\mathcal{A}_e(n)$ and $\mathcal{A}_g(n)$ are distributions dependent on the field number state n associated with the excited and ground states, respectively. A measurement on the two-level atom filters state $|\psi(t)\rangle_{\text{JC}}$ into one of the distributions $\mathcal{A}_e(n)$ or $\mathcal{A}_g(n)$ [40]. Subsequent cycles of unitary dynamics and measurements further narrow the field distribution. Consequently, performing additional sequential measurements on the probe does not significantly improve the gain of information regarding the temperature. In fact, with $n_{\text{seq}} \gg 1$, the resulting state would be purified into a quantum state spanned by only a few field excitations.

C. Intermediate thermalization regime

While previous thermalization regimes show some limited benefits, the question on quantum thermometry is ultimately constrained due to the heat capacity of the probe (strong thermalization regime) and the purification of the probe (weak thermalization regime). Intuitively, leaving the probe to compete between these two cases might harness the sequential measurement thermometry more efficiently, giving rise to surpassing the thermometry achieved by energy measurements over the entire system. To demonstrate the conditions under which sequential thermometry surpasses optimal thermometry strategies, we analyze various figures of merit. Specifically, we examine

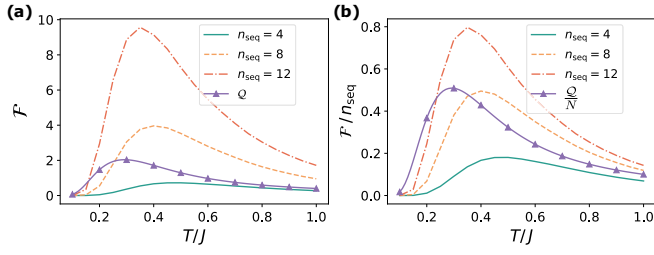


FIG. 6. The Heisenberg probe case. (a) Classical Fisher information \mathcal{F} as a function of temperature T for various numbers of sequential measurements n_{seq} . For comparison, we also plot the quantum Fisher information \mathcal{Q} of the whole spin chain at equilibrium as a function of temperature T . (b) Classical Fisher information \mathcal{F} per sequential measurement n_{seq} as a function of temperature T for several values of n_{seq} . For comparison, we show the quantum Fisher information \mathcal{Q} divided by the system size N (standard thermometry precision per site). Other values are $\kappa = 0.5J$, $N = 4$, and $J\tau = N$.

the rescaled thermometry information per measurement and its behavior as the number of sequential measurements increases.

Let us first consider the Heisenberg many-body probe. In Fig. 6(a), we plot the classical Fisher information as a function of temperature T for several numbers of sequential measurements n_{seq} for a thermalization strength $\kappa = 0.5J$. We consider $J\tau = N$ as the time in between consecutive measurements, with $N = 4$. As seen from the figure, with an increasing number of sequential measurements n_{seq} , the resulting Fisher information increases across all the temperature points. Remarkably, the classical Fisher information obtained through the sequential measurement protocol highly exceeds the quantum Fisher information \mathcal{Q} achieved with equilibrium probes with just a few ($n_{\text{seq}} \sim 8$) sequential measurements. This highlights the remarkable power of sequential measurements in thermometry: with a few undemanding measurements on the local spin, one can achieve precision surpassing that of equilibrium probes, which may require challenging energy measurements with full probe accessibility.

One might argue that the increased number of sequential measurements is responsible for surpassing the thermometry precision achieved by probes at equilibrium. This argument is based on the fact that sequential measurements involve measuring a single local spin multiple times, whereas standard thermometry with probes at equilibrium involves measuring the entire spin chain only once. To address this concern, we consider the sensitivity per measurement. Specifically, we use $\mathcal{F}/n_{\text{seq}}$, which is the classical Fisher information obtained from sequential measurements divided by the number of sequential measurements. For comparison, we use \mathcal{Q}/N , which is the quantum Fisher information of the probe at equilibrium divided by the system size N (standard thermometry precision per site). This comparison provides a fairer

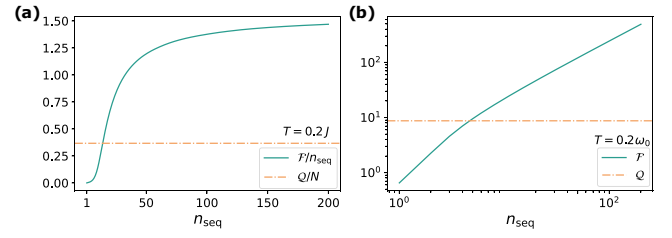


FIG. 7. Asymptotic sensing behavior of the two models. (a) Heisenberg probe: classical Fisher information per measurement as a function of n_{seq} for a given temperature. (b) Jaynes-Cummings model: classical Fisher information as a function of n_{seq} for a given temperature.

assessment of the thermometry precision. In Fig. 6(b), we plot the precision per measurement, $\mathcal{F}/n_{\text{seq}}$ and \mathcal{Q}/N , as a function of the temperature T for several choices of n_{seq} . As seen from the figure, in this normalized scenario, the conclusion holds: sequential measurement thermometry surpasses the thermometry precision achieved by standard thermometry with probes at equilibrium for some specific temperatures and n_{seq} . In particular, it can be observed that, for $n_{\text{seq}} \gtrsim 10$, sequential measurement thermometry outperforms the standard thermometry scheme for a wide range of temperatures.

It has been previously reported that in the asymptotic limit of sequential measurements n_{seq} , the classical Fisher information scales linearly with n_{seq} [101]. Recently, a transition from nonlinear to linear scaling behavior has been explored via Monte Carlo analysis [40]. In the current thermometry scenario, within the intermediate thermalization regime, the probe dynamically encodes the unknown temperature over time, making the question of asymptotic behavior particularly pertinent. In Fig. 7, we plot the classical Fisher information per site as a function of n_{seq} for a given temperature, and we have also included the quantum Fisher information per site for reference. The latter accounts for the rescaled thermometry strategy for a probe in thermal equilibrium. In Fig. 7(a), we consider the Heisenberg probe for the case of $n_{\text{seq}} \gg 1$. As the figure shows, as the probe is constantly thermalized over time, one can still acquire some small information with an extra sequential measurement. However, as the number of sequential measurements becomes increasingly large, such a gain in information becomes more and more modest, as expected from the combination of the mixing channel [101] and the probe's loss of memory of earlier states [40]. Similarly, in Fig. 7(b), we present the asymptotic sensing behavior for the Jaynes-Cummings model, from which similar conclusions are drawn. Note that the Jaynes-Cummings model involves a single qubit; therefore, no rescaling analysis is provided. Moreover, for the parameters considered, the Jaynes-Cummings probe saturates more quickly due to the previously discussed filtering

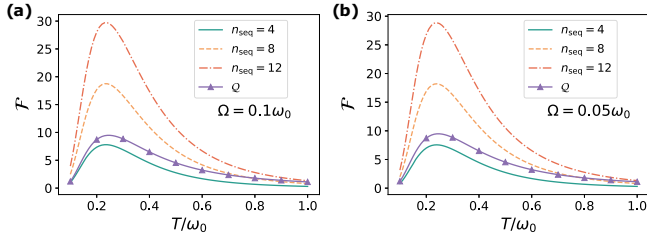


FIG. 8. Jaynes-Cummings probe: classical Fisher information as a function of temperature T for several values of n_{seq} with $\Omega = 0.1\omega_0$ in panel (a) and $\Omega = 0.05\omega_0$ in panel (b). The evolution time between measurements is set to $\omega_0\tau = 20$ and $\kappa = 0.05\omega_0$.

of the Fock distributions from consecutive qubit projections. Interestingly, Figs. 7(a) and 7(b) show that in the large limit of sequential measurements, the thermometry achieved by a sequential measurement strategy can surpass the thermometry achieved with probes at thermal equilibrium.

To further demonstrate the generality of the sequential measurement thermometry scheme outperforming standard thermometry with probes at equilibrium, we consider the Jaynes-Cummings model in the intermediate thermalization regime. In Figs. 8(a) and 8(b), we plot the classical Fisher information as a function of temperature T for several values of n_{seq} with $\Omega = 0.1\omega_0$ in panel (a) and $\Omega = 0.05\omega_0$ in panel (b). For comparison, we also plot the quantum Fisher information of the Jaynes-Cummings probe at thermal equilibrium. As clearly shown in the figure, for both light-matter coupling cases ($\Omega = 0.1\omega_0$ and $\Omega = 0.05\omega_0$), sequential measurement thermometry outperforms most of the standard thermometry scenarios with probes at equilibrium with as few as $n_{\text{seq}} \gtrsim 8$ sequential measurements.

The analysis so far, including a fairer comparison with rescaled figures of merit, clearly demonstrates the benefit of employing sequential thermometry strategies over optimal strategies with probes at thermal equilibrium under

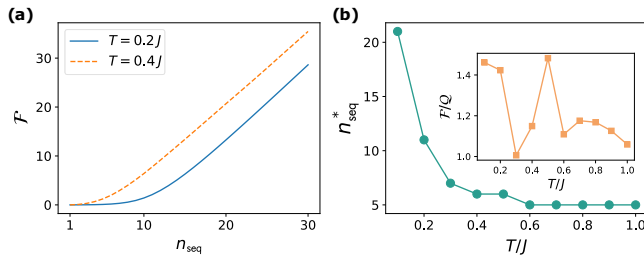


FIG. 9. Heisenberg probe: (a) classical Fisher information \mathcal{F} as a function of n_{seq} for different temperatures, (b) the number of sequential measurements n_{seq}^* needed to exceed the quantum Fisher information obtained by probes at equilibrium as a function of temperature T . The inset in (b) depicts the ratio \mathcal{F}/Q between the classical Fisher information \mathcal{F} at the number of measurements n_{seq}^* over the quantum Fisher information Q . Other values are $\kappa = 0.5J$, $N = 4$, and $J\tau = N$.

certain conditions. One clear aspect is the existence of a specific number of sequential measurements, in the intermediate thermalization regime, where the sequential thermometry strategy proves to exhibit higher accuracy compared to optimal thermometry strategies. To determine the minimum number of sequential measurements n_{seq}^* (for the Heisenberg probe) needed to surpass the optimal thermometry precision achieved by probes at equilibrium, in Fig. 9(a), we plot the classical Fisher information \mathcal{F} as a function of the number of sequential measurements n_{seq} at several temperatures. As shown in the figure, a clear nonlinear behavior for a short number of sequential measurements n_{seq} is observed, while a linear trend with respect to n_{seq} is exhibited as n_{seq} increases. Most notably, in Fig. 9(b) we quantify the minimum number of sequential measurements n_{seq}^* needed to surpass the optimal thermometry precision achieved in energy measurements with full accessibility. As seen from the figure, for the temperature range $0.1J \leq T \leq 1.0J$, the needed number of sequential measurements n_{seq}^* increases (decreases) as the temperature decreases (increases). This can be understood as in the limit towards $T \rightarrow 0$, the Gibbs state will be an eigenstate of the system, namely, the spins parallel to each other (the triplet state).

To quantify the advantage of a probe subjected to sequential measurement thermometry over a thermalized probe with energy measurements, we consider the ratio \mathcal{F}/Q . Here, \mathcal{F} represents the classical Fisher information obtained with the minimum number of sequential measurements n_{seq}^* required to exceed the quantum Fisher information Q obtained from the equilibrium probe. In the inset of Fig. 9(b), by performing n_{seq}^* sequential measurements, one could surpass the quantum Fisher information by about 20% for most of the temperatures shown in the inset of Fig. 9(b).

VI. SIGNAL-TO-NOISE ANALYSIS

From an experimental standpoint, it is a well-known fact that small signals are hard to detect. This is because, in such scenarios, even a small uncertainty in estimating the signal may result in large relative error. To quantify this issue, one can use the signal-to-noise ratio, which is defined as

$$R_\lambda = \frac{\lambda^2}{\text{var}[\hat{\lambda}]}, \quad (31)$$

where λ is the unknown parameter to be estimated and $\text{var}[\hat{\lambda}]$ is the variance of $\hat{\lambda}$ extracted from an unbiased estimator. By using the Cramér-Rao inequality, see Eq. (1), one readily obtains

$$R_\lambda \leq M\lambda^2\mathcal{F}. \quad (32)$$

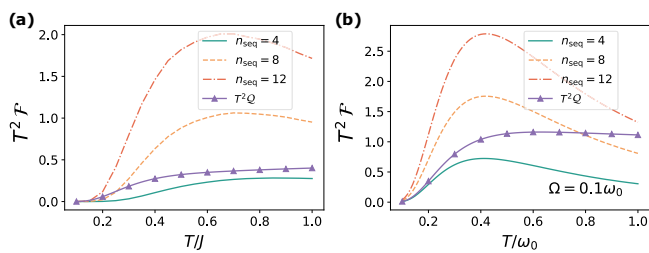


FIG. 10. Signal-to-noise ratio $T^2 \mathcal{F}$ as a function of temperature T for several choices of sequential measurements n_{seq} . For comparison, we also include the signal-to-noise ratio for the optimal thermometry strategy \mathcal{Q} , which involves measuring the entire probe in the energy basis. (a) Heisenberg probe, (b) Jaynes-Cummings probe.

By setting $M = 1$, one can get the single-shot signal-to-noise ratio as a figure of merit for quantifying the quality of sensing. In the above, \mathcal{F} is the classical Fisher information with respect to λ . A good estimability of λ will give higher values of R_λ , namely, $\lambda^2 > \text{var}[\hat{\lambda}]$, for a given value of λ . In Fig. 10, we plot the single-shot signal-to-noise ratio $T^2 \mathcal{F}$ as a function of temperature T for several choices of n_{seq} , when the probe operates in the intermediate thermalization regime. For comparison, we also include the signal-to-noise ratio for the optimal thermometry strategy \mathcal{Q} , which involves measuring the entire probe in the energy basis. In Fig. 10(a), we plot the signal-to-noise ratio for sequential measurement thermometry using the Heisenberg probe. The figure shows that the signal-to-noise ratio increases with the number of sequential measurements n_{seq} . Note that this represents the signal-to-noise ratio for a single measurement $M = 1$, with typical experimental values for measuring a probe of the order of $M \sim 10^3$. It is known that a relationship between the confidence interval and the number of total measurements M can be established using the signal-to-noise ratio [36]. Hence, as shown in Fig. 10(a), the performance of the estimability of T across several values of T becomes higher as n_{seq} increases. On the other hand, as the temperature T decreases, estimating the parameter becomes increasingly challenging. This is because the heat capacity of the probe approaches zero as T decreases. For completeness, in Fig. 10(b), we present the signal-to-noise ratio for sequential measurement thermometry using the Jaynes-Cummings probe, from which similar conclusions can be drawn. Nonetheless, as shown in the figure, the estimability performance is higher across all values of T compared with the Heisenberg probe.

Note that our scheme is minimal, i.e., no optimization on the scheme is performed. Improvement upon optimizing our scheme using quantum control and feedback control can improve the minimal n_{seq} to surpass optimal thermometry in the energy basis. Indeed, under certain conditions, surpassing of the conventional optimal thermometry bound via local undemanding measurements using sequential measurement thermometry is the main result of our work.

VII. CONCLUSIONS

The estimation of temperature has primarily been explored at equilibrium and within the conventional quantum parameter estimation scheme, where a probe is reset after each measurement. In this work, we introduce two main differences: (i) we employ a sequential measurement scheme in which the probe will effectively be different after each measurement due to wave-function collapse, and (ii) we exploit nonequilibrium dynamics to enhance thermometry accuracy. We investigate a many-body probe with Heisenberg interaction in three distinct thermalization scenarios: strong, weak, and intermediate thermalization regimes. Our results reveal that the interplay between quantum state purification from consecutive measurements and thermalization due to reservoir interaction leads to higher thermometry precision as the number of sequential measurements increases. Our results in sequential measurement thermometry show that, under certain conditions, it can surpass the precision achieved by conventional optimal thermometry. Since conventional thermometry often requires energy measurements over the entire system, using consecutive single-qubit measurements may be highly beneficial in practice. This constitutes the main result of our work. To support our claims, we investigate several figures of merit, including thermometry uncertainty bounds, rescaled thermometry information per measurement, and thermometry precision limits for a large number of sequential measurements. All of these metrics demonstrate that, under certain conditions, one can indeed surpass the thermometry capacity of a probe at thermal equilibrium. To further demonstrate the generality of our findings, we also present a light-matter model using the Jaynes-Cummings interaction, which also leads to the same conclusions. Furthermore, our sequential measurement thermometry operates under minimal control constraints. Hence, by fine-tuning parameters such as the evolution time interval, it is feasible to further enhance the protocol's sensitivity.

ACKNOWLEDGMENTS

A.B. acknowledges support from the National Natural Science Foundation of China (Grants No. 12050410253, No. 92065115, and No. 12274059) and the Ministry of Science and Technology of China (Grant No. QNJ2021167001L). V.M. thanks the National Natural Science Foundation of China (Grants No. 12050410251 and No. 12374482).

APPENDIX A: STEADY-STATE VERIFICATION

In this section, we show that the Gibbs state $\rho_{\text{th}} = e^{-H_{\text{Heis}}/T}/\mathcal{Z}(T)$ is indeed the steady state of the Markovian master equation. In particular, we consider the demonstration for the Heisenberg model; for the Jaynes-Cummings

probe, we refer the reader to Ref. [87] for its verification. We demonstrate that (see the main text for details)

$$\begin{aligned}
 0 &= -i[H_{\text{Heis.}}, \rho_{\text{th}}] \\
 &+ \sum_{\substack{j=1 \\ \eta>0}}^N \kappa(\eta) \left[A'_j(\eta) \rho_{\text{th}} A_j^{\dagger}(\eta) - \frac{1}{2} \{A_j^{\dagger}(\eta) A'_j(\eta), \rho_{\text{th}}\} \right] \\
 &+ \sum_{\substack{j=1 \\ \eta>0}}^N \kappa(-\eta) \left[A_j^{\dagger}(\eta) \rho_{\text{th}} A'_j(\eta) - \frac{1}{2} \{A'_j(\eta) A_j^{\dagger}(\eta), \rho_{\text{th}}\} \right].
 \end{aligned} \tag{A1}$$

Recall that the Gibbs state can be written as

$$\rho_{\text{th}} = \frac{1}{\mathcal{Z}(T)} \sum_n e^{-\varepsilon_n/T} |\varepsilon_n\rangle \langle \varepsilon_n|, \tag{A2}$$

where the superscript (j) in $\sigma_+^{(j)} + \sigma_-^{(j)}$ denotes the j th spin, and we have defined $k_{nm}^{(j)} := \langle \varepsilon_n | \sigma_x^{(j)} | \varepsilon_m \rangle$ for simplicity. For a specific Bohr transition η and spin site j , the second and third terms on the right-hand side of Eq. (A1) read

$$\begin{aligned}
 &\kappa(\eta) [A'_j(\eta) \rho(t) A_j^{\dagger}(\eta) - \frac{1}{2} \{A_j^{\dagger}(\eta) A'_j(\eta), \rho(t)\}] + \kappa(-\eta) [A_j^{\dagger}(\eta) \rho(t) A'_j(\eta) - \frac{1}{2} \{A'_j(\eta) A_j^{\dagger}(\eta), \rho(t)\}] \\
 &= \kappa(\eta) k_{nm}^{(j)} k_{nm}^{(j)} [|\varepsilon_n\rangle \langle \varepsilon_m| \rho_{\text{th}} |\varepsilon_m\rangle \langle \varepsilon_n| - \frac{1}{2} (|\varepsilon_m\rangle \langle \varepsilon_m| \rho_{\text{th}} + \rho_{\text{th}} |\varepsilon_m\rangle \langle \varepsilon_m|)] \\
 &+ \kappa(-\eta) k_{nm}^{(j)} k_{mn}^{(j)} [|\varepsilon_m\rangle \langle \varepsilon_n| \rho_{\text{th}} |\varepsilon_n\rangle \langle \varepsilon_m| - \frac{1}{2} (|\varepsilon_n\rangle \langle \varepsilon_n| \rho_{\text{th}} + \rho_{\text{th}} |\varepsilon_n\rangle \langle \varepsilon_n|)].
 \end{aligned} \tag{A6}$$

One can readily calculate the expressions

$$\begin{aligned}
 |\varepsilon_n\rangle \langle \varepsilon_m| \rho_{\text{th}} |\varepsilon_m\rangle \langle \varepsilon_n| &= \frac{1}{\mathcal{Z}(T)} e^{-\varepsilon_m/T} |\varepsilon_n\rangle \langle \varepsilon_n|, \\
 |\varepsilon_m\rangle \langle \varepsilon_n| \rho_{\text{th}} |\varepsilon_n\rangle \langle \varepsilon_m| &= \frac{1}{\mathcal{Z}(T)} e^{-\varepsilon_n/T} |\varepsilon_m\rangle \langle \varepsilon_m|, \\
 \rho_{\text{th}} |\varepsilon_n\rangle \langle \varepsilon_n| &= |\varepsilon_n\rangle \langle \varepsilon_n| \rho_{\text{th}} = \frac{1}{\mathcal{Z}(T)} e^{-\varepsilon_n/T} |\varepsilon_n\rangle \langle \varepsilon_n|.
 \end{aligned}$$

By substituting the above expressions into Eq. (A6), we get

$$\begin{aligned}
 &k_{nm}^{(j)} k_{mn}^{(j)} \kappa(\eta) \frac{e^{-\varepsilon_m/T}}{\mathcal{Z}(T)} [|\varepsilon_n\rangle \langle \varepsilon_n| - |\varepsilon_m\rangle \langle \varepsilon_m|] \\
 &+ k_{nm}^{(j)} k_{mn}^{(j)} \kappa(-\eta) \frac{e^{-\varepsilon_n/T}}{\mathcal{Z}(T)} [|\varepsilon_m\rangle \langle \varepsilon_m| - |\varepsilon_n\rangle \langle \varepsilon_n|].
 \end{aligned} \tag{A7}$$

Now, we impose the KMS condition [87,88], namely,

$$\kappa(-\eta) = \exp\left(\frac{\varepsilon_n - \varepsilon_m}{T}\right) \kappa(\eta). \tag{A8}$$

By substituting the above KMS condition into Eq. (A7), the expression becomes zero. Therefore, the thermal state

where the ε_n are the eigenvalues and the $|\varepsilon_n\rangle$ are the eigenvectors of the Heisenberg Hamiltonian $H_{\text{Heis.}}$. It is then straightforward to show the first term on the right-hand side of Eq. (A1) to be

$$-i[H_{\text{Heis.}}, \rho_{\text{th}}] = 0. \tag{A3}$$

The dissipation terms, namely, the jump operators on the right-hand side of Eq. (A1), are

$$\begin{aligned}
 A'_j(\eta = \varepsilon_m - \varepsilon_n) &= |\varepsilon_n\rangle \langle \varepsilon_n| (\sigma_+^{(j)} + \sigma_-^{(j)}) |\varepsilon_m\rangle \langle \varepsilon_m| \\
 &= \langle \varepsilon_n | \sigma_x^{(j)} | \varepsilon_m \rangle |\varepsilon_n\rangle \langle \varepsilon_m| \\
 &= k_{nm}^{(j)} |\varepsilon_n\rangle \langle \varepsilon_m|,
 \end{aligned} \tag{A4}$$

$$A_j^{\dagger}(\eta = \varepsilon_m - \varepsilon_n) = k_{mn}^{(j)} |\varepsilon_m\rangle \langle \varepsilon_n|, \tag{A5}$$

$\rho_{\text{th}} = e^{-H_{\text{Heis.}}/T} / \mathcal{Z}(T)$ is indeed the steady state of the considered master equation, as required.

APPENDIX B: TEMPERATURE ESTIMATION WITH THE HEISENBERG PROBE

The classical Fisher information determines the sensitivity of an unknown parameter, such as temperature, for a specific POVM. Thus, it represents the bound achievable for a particular measurement basis. However, this bound does not, in actuality, provide the uncertainty of an estimated value. To complete the estimation procedure, it is necessary to input the collected measurement data into an estimator. This maps the collected data into the parameter space [36], providing the actual uncertainty of the estimated value. To demonstrate the actual temperature uncertainty of our sequential measurement thermometry protocol, we use a Bayesian estimator that takes the (correlated) collected data from each quantum trajectory of length n_{seq} and provides an estimated temperature. The Bayes' rule is formulated as

$$P(T|\Gamma) = \frac{P(\Gamma|T)P(T)}{P(\Gamma)}, \tag{B1}$$

where $P(T|\mathbf{\Gamma})$, known as the *posterior*, is the conditional probability for temperature T given a set of measurement outcomes $\mathbf{\Gamma}$; $P(T)$ represents the *prior* information about the unknown temperature T —for the sake of simplicity, we assume that the prior is uniformly distributed— $P(\mathbf{\Gamma}|T)$, known as the *likelihood*, is the conditional probability for the measurement outcomes $\mathbf{\Gamma}$, assuming the unknown parameter T ; and, finally, the denominator $P(\mathbf{\Gamma})$ is a normalization factor such that the posterior is a valid probability distribution, namely, $\int_{T'} P(T'|\mathbf{\Gamma}) dT' = 1$.

In sequential measurement sensing, the observed data of M trajectories are a collection of quantum trajectories given by

$$\mathbf{\Gamma} = \{\boldsymbol{\gamma}_1, \boldsymbol{\gamma}_2, \dots, \boldsymbol{\gamma}_M\}, \quad (\text{B2})$$

where $\mathbf{\Gamma}$ is an array of vector components $\boldsymbol{\gamma}_k$ (representing the k th quantum trajectory), each with n_{seq} spin measurement outcomes, and M is the number of times the probe has been reset. The likelihood function then considers the probable occurrence of each quantum trajectory in the M resetting runs as [39]

$$P(\mathbf{\Gamma}|T) = \frac{M!}{k_1! k_2! \dots k_{2^{n_{\text{seq}}}}!} \prod_{j=1}^{2^{n_{\text{seq}}}} [p(\boldsymbol{\gamma}_j|T)]^{k_j}, \quad (\text{B3})$$

where $p(\boldsymbol{\gamma}_j|T)$ is the conditional probability for quantum trajectory $\boldsymbol{\gamma}_j$ assuming T , $k_1, \dots, k_{2^{n_{\text{seq}}}}$ represent the number of times that the sequence $\boldsymbol{\gamma}_1 = (0_1, 0_2, \dots, 0_{n_{\text{seq}}})$ to $\boldsymbol{\gamma}_{2^{n_{\text{seq}}}} = (1_1, 1_2, \dots, 1_{n_{\text{seq}}})$ occurs in the entire sampling data set M . Here, 0_k and 1_k are the σ_z eigenvalues for the k th measurement instance. It is worth emphasizing that $p(\boldsymbol{\gamma}_j|T)$ requires classically simulating the probability distributions for all possible sequences from $\boldsymbol{\gamma}_1$ to $\boldsymbol{\gamma}_{2^{n_{\text{seq}}}}$ over a relevant range of T . This might entail a significant computational cost as n_{seq} increases. We now present the two representative thermometry scenarios addressed in our work, namely, when the probe bath evolves within a vanishingly weak thermalization strength and when the probe bath thermalizes with a finite strength.

Let us start the analysis for the vanishingly weak thermalization strength, i.e., the unitary dynamics limit. In Fig. 11(a), we show the posterior as a function of temperature T for several numbers of sequential measurements n_{seq} . Here, we assume that we want to estimate the unknown (true) temperature of $T = 0.3J$, utilizing $M = 5000$ quantum trajectories (i.e., the probe has been reset $M = 5000$ times). As the figure indicates, the posterior function tends to center around the true value. Most notably, its spread (or variance of the estimated \hat{T} , $\text{var}[\hat{T}]$) becomes narrower, thus explicitly showing a reduction in temperature uncertainty as n_{seq} increases. In Fig. 11(b), we compare the variance of the temperature $\text{var}[\hat{T}]$ and the inverse of the classical Fisher information \mathcal{F}^{-1} as a function of n_{seq} . We aim to estimate a true (unknown) temperature of $T = 0.3J$ using a sampling of $M = 5000$ quantum trajectories. The system size is set to $N = 8$.

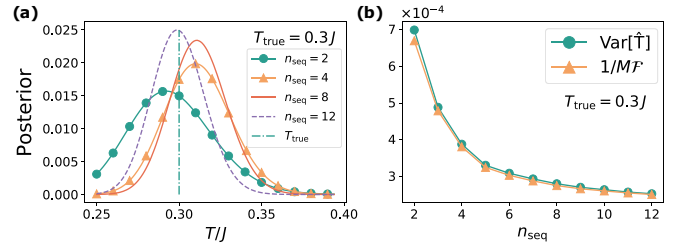


FIG. 11. The unitary dynamics limit. (a) Posterior as a function of temperature T for different numbers of sequential measurements n_{seq} . (b) Comparison between the variance of the temperature estimation $\text{var}[\hat{T}]$ and the inverse of the classical Fisher information \mathcal{F}^{-1} as a function of n_{seq} . We aim to estimate a true (unknown) temperature of $T = 0.3J$ using a sampling of $M = 5000$ quantum trajectories. The system size is set to $N = 8$.

a function of the number of sequential measurements n_{seq} . As seen from the figure, with increasing n_{seq} , the uncertainty of temperature reduces significantly, with the saturation in agreement with the purification of the system due to the consecutive measurements performed on the probe [see the discussion in Sec. VB]. Remarkably, with a finite number of samples $M = 5000$, the variance and the inverse of the classical Fisher information almost overlap, demonstrating both the saturation of the Cramér-Rao inequality $M\text{var}[\hat{T}] \approx \mathcal{F}^{-1}$ and the efficiency of the chosen Bayesian estimation in the presence of correlated measurement outcomes.

In the case of open dynamics with finite thermalization strength, we have demonstrated that the intermediate thermalization regime leads to enhanced thermometry capabilities—see Sec. VC for details. To further illustrate temperature estimation using the Bayesian estimation

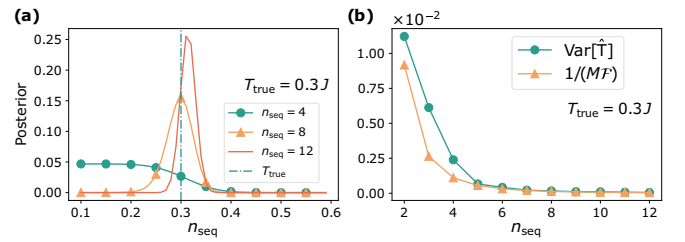


FIG. 12. Open dynamics in the presence of finite probe-bath thermalization strength. (a) Posterior as a function of temperature T for different numbers of sequential measurements n_{seq} . (b) Comparison between the variance of the temperature estimation $\text{var}[\hat{T}]$ and the inverse of the classical Fisher information \mathcal{F}^{-1} as a function of n_{seq} . We aim to estimate a true (unknown) temperature of $T = 0.3J$ using a sample size of $M = 500$ quantum trajectories. Note that in this scenario the posterior is narrower than in the unitary dynamics case [see Fig. 11(a)], remarkably achieved using a smaller number of quantum trajectory samples. Other parameters are $N = 4$ and $\kappa(\omega) = \kappa = 0.5J$.

method, in Fig. 12(a), we show the posterior as a function of temperature T for various numbers of sequential measurements n_{seq} . Here, $T = 0.3J$ represents the true unknown temperature, and we consider $M = 500$ quantum trajectories. As the figure illustrates, two important observations can be made from the posterior function: (i) the posterior peaks at higher values, resulting in a significant reduction in the uncertainty of the temperature; and (ii) this reduction in uncertainty can be achieved with a lower number of quantum trajectories, specifically $M = 500$, which is one order of magnitude less compared to the unitary dynamics case with $M = 5000$. To explicitly observe such a reduction in temperature uncertainty, in Fig. 12(b), we compare the variance of the temperature estimation $\text{var}[T]$ with the inverse of the classical Fisher information \mathcal{F}^{-1} as functions of n_{seq} . As seen from the figure, one achieves $M\text{var}[T] \approx \mathcal{F}^{-1}$ with significantly fewer required quantum trajectories. This observation indicates that allowing the system to thermalize in the intermediate thermalization regime gives rise to an enhanced estimation of the temperature.

-
- [1] A. De Pasquale and T. M. Stace, in *Thermodynamics in the Quantum Regime* (Springer, New York, 2018), pp. 503–527.
- [2] M. Mehboudi, A. Sanpera, and L. A. Correa, Thermometry in the quantum regime: Recent theoretical progress, *J. Phys. A: Math. Theor.* **52**, 303001 (2019).
- [3] M. Quintanilla, M. Henriksen-Lacey, C. Renero-Lecuna, and L. M. Liz-Marzán, Challenges for optical nanothermometry in biological environments, *Chem. Soc. Rev.* **51**, 4223 (2022).
- [4] C. D. S. Brites, P. P. Lima, N. J. O. Silva, A. Millán, V. S. Amaral, F. Palacio, and L. D. Carlos, Thermometry at the nanoscale, *Nanoscale* **4**, 4799 (2012).
- [5] G. Kucsko, P. C. Maurer, N. Y. Yao, M. Kubo, H. J. Noh, P. K. Lo, H. Park, and M. D. Lukin, Nanometre-scale thermometry in a living cell, *Nature* **500**, 54 (2013).
- [6] M. Fujiwara and Y. Shikano, Diamond quantum thermometry: from foundations to applications, *Nanotechnology* **32**, 482002 (2021).
- [7] L. Đačanin Far and M. D. Dramićanin, Luminescence thermometry with nanoparticles: A review, *Nanomaterials* **13**, 2904 (2023).
- [8] Y. Chu and J. Cai, Thermodynamic principle for quantum metrology, *Phys. Rev. Lett.* **128**, 200501 (2022).
- [9] H.-L. Huang, D. Wu, D. Fan, and X. Zhu, Superconducting quantum computing: A review, *Sci. China Inf. Sci.* **63**, 180501 (2020).
- [10] M. Ahumada, F. A. Cárdenas-López, G. Alvarado Barrios, F. Albarrán-Arriagada, and J. C. Retamal, Embedded quantum correlations in thermalized quantum Rabi systems, *Phys. Rev. A* **108**, 012433 (2023).
- [11] H.-G. Xu, V. Montenegro, G. Xianlong, J. Jin, and G. D. d. M. Neto, Persisting quantum effects in the anisotropic Rabi model at thermal equilibrium, *Phys. Rev. Res.* **6**, 013001 (2024).
- [12] T. P. Purdy, P.-L. Yu, N. S. Kampel, R. W. Peterson, K. Cicak, R. W. Simmonds, and C. A. Regal, Optomechanical Raman-ratio thermometry, *Phys. Rev. A* **92**, 031802 (2015).
- [13] V. Montenegro, M. G. Genoni, A. Bayat, and M. G. A. Paris, Mechanical oscillator thermometry in the nonlinear optomechanical regime, *Phys. Rev. Res.* **2**, 043338 (2020).
- [14] S. Razavian, C. Benedetti, M. Bina, Y. Akbari-Kourbolagh, and M. G. A. Paris, Quantum thermometry by single-qubit dephasing, *Eur. Phys. J. Plus* **134**, 284 (2019).
- [15] D. Burgarth, V. Giovannetti, A. N. Kato, and K. Yuasa, Quantum estimation via sequential measurements, *New J. Phys.* **17**, 113055 (2015).
- [16] E. O'Connor, S. Campbell, and G. T. Landi, Fisher information rates in sequentially measured quantum systems, *New J. Phys.* **26**, 033048 (2024).
- [17] G. Mihailescu, S. Campbell, and A. K. Mitchell, Thermometry of strongly correlated fermionic quantum systems using impurity probes, *Phys. Rev. A* **107**, 042614 (2023).
- [18] G. Mihailescu, A. Bayat, S. Campbell, and A. K. Mitchell, Multiparameter critical quantum metrology with impurity probes, *Quantum Sci. Technol.* **9**, 035033 (2024).
- [19] A. K. Srivastava, U. Bhattacharya, M. Lewenstein, and M. Płodzień, Topological quantum thermometry, [ArXiv:2311.14524](https://arxiv.org/abs/2311.14524).
- [20] M. Płodzień, R. Demkowicz-Dobrzański, and T. Sowiński, Few-fermion thermometry, *Phys. Rev. A* **97**, 063619 (2018).
- [21] P. Sekatski and M. Perarnau-Llobet, Optimal nonequilibrium thermometry in Markovian environments, *Quantum* **6**, 869 (2022).
- [22] L. A. Correa, M. Mehboudi, G. Adesso, and A. Sanpera, Individual quantum probes for optimal thermometry, *Phys. Rev. Lett.* **114**, 220405 (2015).
- [23] V. Mukherjee, A. Zwick, A. Ghosh, X. Chen, and G. Kurizki, Enhanced precision bound of low-temperature quantum thermometry via dynamical control, *Commun. Phys.* **2**, 162 (2019).
- [24] J. Glatthard, J. Rubio, R. Sawant, T. Hewitt, G. Barontini, and L. A. Correa, Optimal cold atom thermometry using adaptive Bayesian strategies, *PRX Quantum* **3**, 040330 (2022).
- [25] W.-K. Mok, K. Bharti, L.-C. Kwek, and A. Bayat, Optimal probes for global quantum thermometry, *Commun. Phys.* **4**, 62 (2021).
- [26] J. Rubio, J. Anders, and L. A. Correa, Global quantum thermometry, *Phys. Rev. Lett.* **127**, 190402 (2021).
- [27] S. Campbell, M. Mehboudi, G. D. Chiara, and M. Paterostro, Global and local thermometry schemes in coupled quantum systems, *New J. Phys.* **19**, 103003 (2017).
- [28] G. O. Alves and G. T. Landi, Bayesian estimation for collisional thermometry, *Phys. Rev. A* **105**, 012212 (2022).
- [29] M. R. Jørgensen, J. Kołodyński, M. Mehboudi, M. Perarnau-Llobet, and J. B. Brask, Bayesian quantum thermometry based on thermodynamic length, *Phys. Rev. A* **105**, 042601 (2022).

- [30] L. Ostermann and K. Gietka, Temperature-enhanced critical quantum metrology, *Phys. Rev. A* **109**, L050601 (2024).
- [31] E. Aybar, A. Niezgodá, S. S. Mirkhalaf, M. W. Mitchell, D. Benedicto Orenes, and E. Witkowska, Critical quantum thermometry and its feasibility in spin systems, *Quantum* **6**, 808 (2022).
- [32] A. Ullah, M. T. Naseem, and O. E. Müstecaplıođlu, Low-temperature quantum thermometry boosted by coherence generation, *Phys. Rev. Res.* **5**, 043184 (2023).
- [33] M. Mehboudi, M. R. Jørgensen, S. Seah, J. B. Brask, J. Kołodyński, and M. Perarnau-Llobet, Fundamental limits in Bayesian thermometry and attainability via adaptive strategies, *Phys. Rev. Lett.* **128**, 130502 (2022).
- [34] T. Jahnke, S. Lanéry, and G. Mahler, Operational approach to fluctuations of thermodynamic variables in finite quantum systems, *Phys. Rev. E* **83**, 011109 (2011).
- [35] T. M. Stace, Quantum limits of thermometry, *Phys. Rev. A* **82**, 011611 (2010).
- [36] M. G. Paris, Quantum estimation for quantum technology, *Int. J. Quantum Inf.* **7**, 125 (2009).
- [37] K. V. Hovhannisyán, M. R. Jørgensen, G. T. Landi, Á. M. Alhambra, J. B. Brask, and M. Perarnau-Llobet, Optimal quantum thermometry with coarse-grained measurements, *PRX Quantum* **2**, 020322 (2021).
- [38] J. Glatthard, K. V. Hovhannisyán, M. Perarnau-Llobet, L. A. Correa, and H. J. D. Miller, Energy measurements remain thermometrically optimal beyond weak coupling, *Quantum* **7**, 1190 (2023).
- [39] V. Montenegro, G. S. Jones, S. Bose, and A. Bayat, Sequential measurements for quantum-enhanced magnetometry in spin chain probes, *Phys. Rev. Lett.* **129**, 120503 (2022).
- [40] Y. Yang, V. Montenegro, and A. Bayat, Extractable information capacity in sequential measurements metrology, *Phys. Rev. Res.* **5**, 043273 (2023).
- [41] P. Busch, G. Cassinelli, and P. J. Lahti, On the quantum theory of sequential measurements, *Found. Phys.* **20**, 757 (1990).
- [42] H.-J. Schmidt and J. Gemmer, Sequential measurements and entropy, *J. Phys.: Conf. Ser.* **1638**, 012007 (2020).
- [43] M. Ban, On sequential measurements with indefinite causal order, *Phys. Lett. A* **403**, 127383 (2021).
- [44] B. Skinner, J. Ruhman, and A. Nahum, Measurement-induced phase transitions in the dynamics of entanglement, *Phys. Rev. X* **9**, 031009 (2019).
- [45] M. Block, Y. Bao, S. Choi, E. Altman, and N. Y. Yao, Measurement-induced transition in long-range interacting quantum circuits, *Phys. Rev. Lett.* **128**, 010604 (2022).
- [46] T. Benoist, J.-L. Fatras, and C. Pellegrini, Limit theorems for quantum trajectories, *Stoch. Process Their. Appl.* **164**, 288 (2023).
- [47] E. Haapasalo, T. Heinosaari, and Y. Kuramochi, Saturation of repeated quantum measurements, *J. Phys. A: Math. Theor.* **49**, 33LT01 (2016).
- [48] T. Benoist, M. Fraas, Y. Pautrat, and C. Pellegrini, Invariant measure for quantum trajectories, *Probab. Theory Relat. Fields* **174**, 307 (2019).
- [49] D. K. Burgarth, P. Facchi, V. Giovannetti, H. Nakazato, S. Pascazio, and K. Yuasa, Exponential rise of dynamical complexity in quantum computing through projections, *Nat. Commun.* **5**, 1 (2014).
- [50] S. Pouyandeh, F. Shahbazi, and A. Bayat, Measurement-induced dynamics for spin-chain quantum communication and its application for optical lattices, *Phys. Rev. A* **90**, 012337 (2014).
- [51] A. Bayat, B. Alkurtass, P. Sodano, H. Johannesson, and S. Bose, Measurement quench in many-body systems, *Phys. Rev. Lett.* **121**, 030601 (2018).
- [52] W.-L. Ma, P. Wang, W.-H. Leong, and R.-B. Liu, Phase transitions in sequential weak measurements, *Phys. Rev. A* **98**, 012117 (2018).
- [53] T. Rybár and M. Ziman, Process estimation in the presence of time-invariant memory effects, *Phys. Rev. A* **92**, 042315 (2015).
- [54] H. Mabuchi, Dynamical identification of open quantum systems, *Quantum Semiclassical Opt.: J. Eur. Opt. Soc. Part B* **8**, 1103 (1996).
- [55] A. De Pasquale, K. Yuasa, and V. Giovannetti, Estimating temperature via sequential measurements, *Phys. Rev. A* **96**, 012316 (2017).
- [56] A. Ritboon, L. Slodička, and R. Filip, Sequential phonon measurements of atomic motion, *Quantum Sci. Technol.* **7**, 015023 (2022).
- [57] M. Bompais and N. Amini, in *2023 62nd IEEE Conference on Decision and Control (CDC)* (IEEE, Singapore, 2023), p. 5926.
- [58] M. Bompais, N. H. Amini, and C. Pellegrini, in *2022 IEEE 61st Conference on Decision and Control (CDC)* (Cancún, Mexico, 2022), p. 5161.
- [59] S. Gherardini, A. Smirne, M. M. Müller, and F. Caruso, Advances in sequential measurement and control of open quantum systems, *Proceedings* **12**, 11 (2019).
- [60] J. Gambetta and H. M. Wiseman, State and dynamical parameter estimation for open quantum systems, *Phys. Rev. A* **64**, 042105 (2001).
- [61] M. M. Müller, S. Gherardini, A. Smerzi, and F. Caruso, Fisher information from stochastic quantum measurements, *Phys. Rev. A* **94**, 042322 (2016).
- [62] E. Nagali, S. Felicetti, P.-L. de Assis, V. D’Ambrosio, R. Filip, and F. Sciarrino, Testing sequential quantum measurements: How can maximal knowledge be extracted?, *Sci. Rep.* **2**, 443 (2012).
- [63] A. H. Kiilerich and K. Mølmer, Quantum zeno effect in parameter estimation, *Phys. Rev. A* **92**, 032124 (2015).
- [64] L. A. Clark, A. Stokes, and A. Beige, Quantum jump metrology, *Phys. Rev. A* **99**, 022102 (2019).
- [65] M. Radaelli, G. T. Landi, K. Modi, and F. C. Binder, Fisher information of correlated stochastic processes, *New J. Phys.* **25**, 053037 (2023).
- [66] A. S. Holevo, in *Quantum Probability and Applications to the Quantum Theory of Irreversible Processes* (Springer, New York, 1984), pp. 153–172.
- [67] H. Cramér, *Mathematical Methods of Statistics* (Princeton University Press, Princeton, 1999), Vol. 26.
- [68] L. M. Le Cam, *Asymptotic Methods in Statistical Decision Theory*, Springer Series in Statistics Springer-Verlag, New York, 1986.
- [69] C. W. Helstrom, Quantum detection and estimation theory, *J. Stat. Phys.* **1**, 231 (1969).

- [70] R. Zamir, A proof of the Fisher information inequality via a data processing argument, *IEEE Trans. Inf. Theory* **44**, 1246 (1998).
- [71] H. Cramer, *Mathematical Methods of Statistics* (Princeton University Press, Princeton, 1946), p. xvi, 575 p.
- [72] C. R. Rao, in *Breakthroughs in Statistics: Foundations and Basic Theory*, edited by S. Kotz and N. L. Johnson (Springer New York, New York, NY, 1992), p. 235.
- [73] C. Helstrom, Minimum mean-squared error of estimates in quantum statistics, *Phys. Lett. A* **25**, 101 (1967).
- [74] H. Yuen and M. Lax, Multiple-parameter quantum estimation and measurement of nonselfadjoint observables, *IEEE Trans. Inf. Theory* **19**, 740 (1973).
- [75] C. Helstrom and R. Kennedy, Noncommuting observables in quantum detection and estimation theory, *IEEE Trans. Inf. Theory* **20**, 16 (1974).
- [76] S. L. Braunstein and C. M. Caves, Statistical distance and the geometry of quantum states, *Phys. Rev. Lett.* **72**, 3439 (1994).
- [77] J. Hájek, A characterization of limiting distributions of regular estimates, *Z. Wahrscheinlichkeit. Verwandte Gebiete* **14**, 323 (1970).
- [78] H. L. van Trees, *Detection, Estimation and Modulation Theory, Part I* (Wiley & Sons, New York, 1968).
- [79] R. D. Gill and B. Y. Levit, Applications of the van Trees inequality: A Bayesian Cramér-Rao bound, *Bernoulli* **1**, 59 (1995).
- [80] V. Montenegro, U. Mishra, and A. Bayat, Global sensing and its impact for quantum many-body probes with criticality, *Phys. Rev. Lett.* **126**, 200501 (2021).
- [81] H.-J. Mikeska and A. K. Kolezhuk, in *Quantum Magnetism*, edited by U. Schollwöck, J. Richter, D. J. J. Farnell, and R. F. Bishop (Springer Berlin Heidelberg, Berlin, Heidelberg, 2004), p. 1.
- [82] A. Bayat and S. Bose, Information-transferring ability of the different phases of a finite XXZ spin chain, *Phys. Rev. A* **81**, 012304 (2010).
- [83] S. Bose, Quantum communication through an unmodulated spin chain, *Phys. Rev. Lett.* **91**, 207901 (2003).
- [84] G. D. Chiara, S. Montangero, P. Calabrese, and R. Fazio, Entanglement entropy dynamics of Heisenberg chains, *J. Stat. Mech.: Theory Exp.* **2006**, P03001 (2006).
- [85] Y. Endoh, G. Shirane, R. J. Birgeneau, P. M. Richards, and S. L. Holt, Dynamics of an $s = \frac{1}{2}$, one-dimensional Heisenberg antiferromagnet, *Phys. Rev. Lett.* **32**, 170 (1974).
- [86] J. Larson and T. Mavrogordatos, *The Jaynes–Cummings Model and Its Descendants: Modern Research Directions* (IOP Publishing, Bristol, 2021).
- [87] M. Scala, B. Militello, A. Messina, J. Piilo, and S. Maniscalco, Microscopic derivation of the Jaynes-Cummings model with cavity losses, *Phys. Rev. A* **75**, 013811 (2007).
- [88] A. Rivas and S. F. Huelga, *Open Quantum Systems* (Springer, Heidelberg, 2012), Vol. 10.
- [89] M. Cattaneo, G. L. Giorgi, S. Maniscalco, and R. Zambrini, Local versus global master equation with common and separate baths: Superiority of the global approach in partial secular approximation, *New J. Phys.* **21**, 113045 (2019).
- [90] V. Eremeev, V. Montenegro, and M. Orszag, Thermally generated long-lived quantum correlations for two atoms trapped in fiber-coupled cavities, *Phys. Rev. A* **85**, 032315 (2012).
- [91] V. Montenegro and M. Orszag, Creation of entanglement of two atoms coupled to two distant cavities with losses, *J. Phys. B: At., Mol. Opt. Phys.* **44**, 154019 (2011).
- [92] V. Montenegro, V. Eremeev, and M. Orszag, Entanglement of two distant qubits driven by thermal environments, *Phys. Scr.* **2012**, 014022 (2012).
- [93] H.-P. Breuer and F. Petruccione, *The Theory of Open Quantum Systems* (Oxford University Press, New York, 2007).
- [94] C.-F. Chen, M. J. Kastoryano, F. G. S. L. Brandão, and A. Gilyén, Quantum thermal state preparation, [ArXiv:2303.18224](https://arxiv.org/abs/2303.18224).
- [95] M. A. Nielsen and I. L. Chuang, *Quantum Computation and Quantum Information* (Cambridge University Press, New York, 2000).
- [96] C. L. Degen, F. Reinhard, and P. Cappellaro, Quantum sensing, *Rev. Mod. Phys.* **89**, 035002 (2017).
- [97] V. Giovannetti, S. Lloyd, and L. Maccone, Advances in quantum metrology, *Nat. Photonics* **5**, 222 (2011).
- [98] V. Giovannetti, S. Lloyd, and L. Maccone, Quantum metrology, *Phys. Rev. Lett.* **96**, 010401 (2006).
- [99] V. Giovannetti, S. Lloyd, and L. Maccone, Quantum-enhanced measurements: Beating the standard quantum limit, *Science* **306**, 1330 (2004).
- [100] H. Maassen and B. Kümmerer, Purification of quantum trajectories, *Lect. Notes-Monogr. Ser.* **48**, 256 (2006).
- [101] D. Burgarth, V. Giovannetti, A. N. Kato, and K. Yuasa, Quantum estimation via sequential measurements, *New J. Phys.* **17**, 113055 (2015).